Top Catal (2017) 60:1276–1284
DOI 10.1007/s11244-017-0812-2

ORIGINAL PAPER

Deactivation of Ni/γ-Al_2O_3 Catalysts in CO Methanation: Effect of Zr, Mg, Ba and Ca Oxide Promoters

Javier Barrientos[1] · Niklas Gonzalez[1] · Magali Boutonnet[1] · Sven Järås[1]

Published online: 30 May 2017

Abstract Catalyst deactivation is one of the major concerns in the production of substitute natural gas (SNG) via CO methanation. Catalysts in this application need to be active at low temperatures, resistant to polymeric carbon formation and stable at high temperatures and steam partial pressures. In the present work, a series of alumina-supported nickel catalysts promoted with Zr, Mg, Ba or Ca oxides were investigated. The catalysts were tested under low temperature CO methanation conditions in order to evaluate their resistance to carbon formation. The catalysts were also exposed to accelerated ageing conditions at high temperatures in order to study their thermal stability. The aged catalysts lost most of their activity mainly due to sintering of the support and the nickel crystallites. Apparently, none of these promoters had a satisfactory effect on the thermal resistance of the catalyst. Nevertheless, it was found that the presence of Zr can reduce the rate of polymeric carbon formation.

Keywords Nickel · Alumina · Promoters · Methanation · Deactivation · SNG

1 Introduction

Production of substitute natural gas (SNG) from coal, biomass or other carbonaceous sources is gaining great attention in areas located far from natural gas or shale gas reserves [1, 2]. The SNG production process involves two steps: gasification of the carbon-containing feedstock and subsequent catalytic methanation of the resulting synthesis gas. Methanation of synthesis gas involves the two following reactions [3–5]:

$$CO + 3H_2 \rightarrow CH_4 + H_2O \ (\Delta H^\circ = -206 \text{ kJ/mol})$$

$$CO_2 + 4H_2 \rightarrow CH_4 + 2H_2O \ (\Delta H^\circ = -165 \text{ kJ/mol})$$

These reactions are thermodynamically favored at low temperature and high pressure [6]. It is therefore that the methanation process is designed to effectively remove the heat of reaction and thus maximize the methane yield [1, 7]. There are currently two main methanation concepts: single fluidized bed reactors and series of adiabatic fixed bed reactors with intercooling [1]. The latter, also known as high temperature methanation, has already found commercial application [8, 9].

Alumina-supported nickel catalysts are usually employed in this application due to their high activity, selectivity to methane and relatively low price [7]. However, their stability is threatened by the severe conditions of the high temperature methanation process [10, 11]. In this process, the catalyst at the inlet of the reactor is exposed to low temperatures and high CO partial pressures, fact that favors the formation of polymeric carbon and sintering via nickel carbonyl formation [4, 12–14]. The exothermic reactions cause a significant temperature rise. As a result, the major part of the catalyst in these reactors is exposed to high temperatures and high steam partial pressures fact that promotes sintering of the nickel nanoparticles and the support [11, 15]. In order to limit the temperature rise and thus, catalyst deactivation, a high gas recycle is used in these reactors. Catalysts with improved stability at low and

✉ Javier Barrientos
javbar@kth.se

[1] KTH (Royal Institute of Technology), Chemical Science and Engineering, Chemical Technology, Teknikringen 42, Plant 6, 100 44 Stockholm, Sweden

high temperatures allow for a larger operating temperature span and thus, diminish gas recycling costs [8].

The thermal stability of a catalyst can be improved by calcining the carrier and/or the catalyst at high temperatures. Yet, high temperature treatments lead to catalysts with low metallic surface area and so, low activity. This problem is presented, for instance, in the work of Gao et al. [16] in which they studied the effect of the alumina calcination temperature prior to its impregnation with the Ni precursor. In their work, they showed that low calcination temperatures lead to high surface area carriers and, consequently, to catalysts with higher nickel dispersion, as expected. Unfortunately, the prepared high surface area catalysts were unstable due to severe sintering of the Ni nanoparticles and partial collapse of the support.

This compromise between catalyst stability and activity was also illustrated in the work of Nguyen et al. [8], in which they showed that Ni crystals can grow from 9 nm to more than 100 nm if high surface area nickel-alumina catalysts are employed. Contrariwise, they showed that the MCR-2X catalyst from Haldor Topsoe [4] presents a considerably more stable performance allowing operation at temperatures as high as 700 °C. The MCR-2X catalyst consists of 22 wt% Ni [11] supported on a pre-stabilized γ-Al_2O_3 support [17]. The reported BET surface area and nickel particle size are approximately 45 m^2/g and 16 nm, respectively [4, 8].

Another possible solution to increase the stability of nickel alumina catalysts is the use of oxide promoters [18]. For instance, several researchers [19–22] have found that addition of ZrO_2 can reduce the formation of carbon and enhance the thermal resistance of both the carrier and the Ni particles. Rotgerink et al. [23] found that the addition of La_2O_3 can restrain the growth of Ni particles. Others [24, 25] have showed that the addition of MgO can improve the thermal stability of the catalyst. To the best of our knowledge, there are no studies investigating the effect of other alkaline earth oxide promoters such as BaO or CaO. According to Alipour et al. [26, 27], doping of γ-Al_2O_3 with BaO and CaO with concentrations as low as 3 wt% can significantly reduce the carbon formation rate in dry methane reforming. Hence, an insight into the effect of these other promoters in CO methanation could be of interest.

The objective of the present work is to evaluate the effect of different structural promoters on carbon formation and thermal sintering under relevant methanation conditions. For that purpose, a high surface area γ-Al_2O_3 carrier was impregnated with salts of Zr, Mg, Ba and Ca. The catalysts were exposed to accelerated ageing conditions at high temperatures and high steam partial pressures in order to evaluate their thermal stability. The catalysts were also tested under low temperature CO methanation conditions in order to analyze and quantify the amount of carbon formed.

2 Experimental

2.1 Catalyst Preparation

The γ-Al_2O_3 carrier employed in the present work was supplied by Saint Gobain NorPro (product type: SA 6173) and consists of cylindrical pellets with a diameter of 3.6 mm and an average length of 5 mm. Prior to impregnation with the promoter salts, the alumina carrier was dried at 120 °C for 6 h and then calcined in flowing air for 10 h at 500 °C (heating rate: 1 °C/min).

The calcined pellets were then impregnated with aqueous solutions of $Zr(NO_3)_2{\cdot}xH_2O$ (Sigma Aldrich, 99%), $Mg(NO_3)_2{\cdot}6H_2O$ (Sigma Aldrich, ACS Reagent 99%), $Ba(NO_3)_2$ (Sigma Aldrich, ACS Reagent 99%) and $Ca(NO_3)_2$ $\cdot 4H_2O$ (Sigma Aldrich, ACS reagent 99%). Approximately 5 g of γ-Al_2O_3 pellets were immersed in a vessel containing 40 mL of the precursor solution during 15 h under stirring. Then, the solution was heated up at 120 °C until its evaporation. Finally the samples were dried at 120 °C for 6 h and calcined in air at 500 °C for 10 h (heating rate: 1 °C/min). A total of 4 carriers were prepared containing 5 wt% of one oxide promoter. These were named "ZrAl, "MgAl", "BaAl" and "CaAl", according to the promoter used in each case. The unpromoted calcined alumina carrier was named "Al".

The supports were then impregnated with Ni using exactly the same impregnation procedure. An aqueous solution of $Ni(NO_3)_2{\cdot}6H_2O$ [puriss. p.a.; ≥98.5% (KT), Fluka] was used for that purpose. After impregnation and evaporation of the precursor solution, the samples were dried at 120 °C for 3 h and calcined in air at 500 °C for 3 h (heating rate: 2.5 °C/min). The resulting catalysts, containing 30 wt% Ni, were named NiAl, NiZrAl, NiMgAl, NiBaAl and NiCaAl, according to the carrier used.

The catalysts and carriers were crushed into a fine powder in order to perform catalytic tests and characterization analyses. The original cylindrical catalyst pellets were only used in the accelerated ageing treatments.

2.2 Catalyst Characterization Techniques

Brunauer-Emmett-Teller (BET) surface area and porosity measurements were performed in a Micromeritics ASAP 2000/2010 unit. The samples were evacuated and dried overnight at 250 °C prior to analysis. The BET surface area was estimated by N_2 adsorption at liquid nitrogen temperature at relative pressures between 0.06 and 0.2. The pore volume was estimated from a single adsorption point at a relative pressure of 0.998. The average pore diameter was estimated from the pore volume and the BET surface area assuming cylindrical pores. The pore size distribution was

calculated with the Barrett–Joyner–Halenda (BJH) method using the desorption isotherm.

X-ray diffraction (XRD) measurements were performed on the unreduced and reduced catalysts as well as on the spent samples in a Siemens D5000 diffractometer with Cu-Kα radiation (2θ = 10°–90°, step size =0.02°) equipped with a Ni filter. The average crystallite diameter of Ni [$d(Ni^0)_{XRD}$, nm] and NiO [$d(NiO)_{XRD}$, nm] were estimated by using the Scherrer formula and assuming that the particles are spherical [28]. The NiO crystal size was estimated using the peak situated in the 2θ range of 62°–65°. The Ni crystal size was estimated using the peak situated between 50°–54°.

Hydrogen temperature-programmed reduction (TPR) was used to study the reducibility of the catalysts. TPR of the calcined samples was performed in a Micromeritics Autochem 2910 by flowing 5% H_2 in Ar and increasing the temperature from ambient to 1000 °C (heating rate: 10 °C/min) while monitoring the H_2 consumption by means of a thermal conductivity detector (TCD). The degree of reduction (DOR, %) was estimated from TPR after in situ reduction of the catalyst at 500 °C for 4 h (heating rate: 5 °C/min) in pure H_2 flow. The DOR was calculated assuming that the unreduced nickel oxide was composed of Ni(II) as evidenced from XRD.

Hydrogen-static chemisorption was performed on the fresh and spent catalysts in order to estimate the nickel dispersion (D_H, %) and the nickel crystallite size [$d(Ni^0)_H$, nm]. The chemisorption measurements were conducted in a Micromeritics ASAP 2020C unit at 35 °C, after in situ reduction of the catalyst at 500 °C for 4 h (heating rate =5 °C/min). The average particle size of Ni was calculated according to [29]:

$$d\left(Ni^0\right)_H = \frac{0.97}{D_H} \times DOR$$

2.3 Low Temperature CO Methanation Tests: Carbon Formation Study

The catalytic tests were performed in a down-flow stainless steel fixed bed reactor (i.d. 9 mm) with a catalyst loading of 100 mg (catalyst pellet size range =53–90 µm) diluted with approximately 4 g of SiC (average pellet size =75 µm). The reaction conditions were: 300 °C (±2 °C), atmospheric pressure and an inlet H_2/CO =3. The tests were performed at atmospheric pressure in order to avoid deactivation due to sintering via nickel carbonyl formation [13]. The same syngas flow (12 NL/h) was used for all the catalytic tests. The syngas feed contained 2% N_2 as an internal standard. At these conditions, the small pellet size used ensured the absence of any mass and heat transfer limitations [14, 30]. The reactor tube was heated by means of an oven and the temperature inside the reactor was regulated by cascade control with one sliding thermocouple in the catalyst bed and another one placed in the oven. A detailed description of the equipment has been given elsewhere [31–33].

Prior to reaction, the catalysts were reduced in situ in pure H_2 flow at atmospheric pressure and 500 °C for 4 h (heating rate =5 °C/min). After reduction, the catalysts were cooled to reaction temperature (300 °C) and then flushed with He before increasing the pressure to the desired level. Afterwards, the methanation experiments started with a stepwise increase of the syngas flow, together with a stepwise decrease of the He flow, in order to avoid a large temperature rise in the catalyst bed due to the exothermic reaction.

The product gases were analyzed on-line by means of a gas chromatograph (GC) Agilent 6890 equipped with a TCD and a flame ionization detector (FID). N_2, CO, CH_4 and CO_2 were separated by a Carbosieve II packed column and analyzed on the TCD. The C1-C4 hydrocarbons were separated by an alumina-plot column and quantified on the FID.

After 24 h, the syngas flow was replaced by helium flow. The reactor was then heated up to 500 °C for 4 h in order to remove any possible weakly adsorbed species on the catalyst surface. Afterwards the reactor was cooled down to room temperature. The carbon species formed on the spent samples were then analyzed and quantified by means of in situ temperature-programmed hydrogenation (TPH) analyses. The TPH analyses were performed by flowing pure H_2 (1.4 NL/h) and increasing the temperature from ambient to 690 °C (ramp: 1 °C/min) while monitoring the methane concentration in H_2.

The methane signal, resulting from the TPH analyses, was monitored with a HiQuadTM QMG700 mass spectrometer (m/z = 15, instead of 16 to avoid the interference of ionized oxygen from water vapor [34]). The pressure in the MS chamber, the SEM voltage and the signal reading duration were set, respectively, at 5×10^{-6} mbar, 2000 kV and 1 s. The gas composition was simultaneously analyzed with the FID in the GC used for the low-temperature CO methanation tests in order to observe if hydrocarbons different than CH_4 form during these TPH analyses.

2.4 Accelerated Ageing Tests: Thermal Sintering Study

The accelerated ageing tests were carried out in the same fixed bed reactor used for the low temperature CO methanation tests. For that purpose, the cylindrical catalyst pellets were all loaded in the reactor and diluted with fine SiC powder (average pellet size =75 µm). The catalysts were aged at 690 °C (±5 °C) with a H_2O/H_2 flow (H_2O/H_2 =2). This accelerated ageing method was also used in the work of Nguyen et al. [8]. Nevertheless, two different

accelerating ageing tests were performed for each catalyst. One test was carried out at 1 bar and another at 30 bars. After 7 days, the H_2O/H_2 flow was replaced by helium flow and the reactor was cooled down to room temperature. Then, the helium flow was stopped and the aged samples were passivated by contact with air. The cylindrical pellets were then crushed into fine powder and analyzed by means of XRD, H_2-chemisorption and N_2 adsorption analyses.

In addition, activity measurements were performed on fresh and aged samples. For that purpose, the catalysts were tested at very mild conditions (300 °C, 1 bar and inlet H_2/CO =9) in order to minimize the deactivation rate and thus, more accurately determine the activity of the samples. This procedure was also used in the work of Nguyen et al. [8]. The tests were carried out in the same reactor used for the low temperature CO methanation tests. The catalyst loading was 50 mg, diluted with 4 g of SiC, and the syngas flow was 12 NL/h.

3 Results and Discussion

3.1 Characterization of the Catalysts and Supports

The physical properties of the carriers and the fresh catalysts after calcination are presented in Table 1. All the samples are characterized by a high surface area. All the catalysts present a monomodal mesopore size distribution in the range of 2–15 nm. The results also suggest that the physical properties of the alumina support are not significantly affected after impregnation of the promoters. Nevertheless, all samples lose surface area and porosity after impregnation with Ni.

Table 1 Physical properties of the carriers and the fresh catalysts

Sample	BET surface area (m^2/g_{cat})	Pore volume (cm^3/g_{cat})	Average pore diameter (nm)[a]
Carriers			
Al	223	0.64	11.5
ZrAl	244	0.67	11.0
MgAl	210	0.59	11.2
BaAl	220	0.57	10.3
CaAl	212	0.58	11.0
Catalysts			
NiAl	176	0.39	8.8
NiZrAl	225	0.52	9.3
NiMgAl	155	0.37	9.6
NiBaAl	190	0.39	8.3
NiCaAl	167	0.32	7.7

[a]Calculated according to: four·pore volume/BET surface area

The TPR profiles of the calcined catalysts are presented in Fig. 1. As can be seen, all the reduction profiles present peaks at different temperatures. The peaks situated between 300 and 400 °C are assigned to the reduction of large NiO crystals weakly bounded to the support [35]. The wide reduction area between 400 and 1000 °C are assigned to the reduction of small NiO crystallites strongly interacting with the support and spinel compounds (e.g. $NiAl_2O_4$) [35–37]. Even though the profiles are similar for all the catalysts, some small differences can be noted. For instance, the NiAl catalyst presents a very large high temperature peak compared to the other catalysts. This difference could be assigned to a slight inhibiting effect of the promoters in the formation of nickel aluminates. Moreover, the NiCaAl catalyst presents the largest low temperature peak. Finally, slightly lower temperatures are required to completely reduce the NiCaAl and NiZrAl catalysts.

The DOR's of the catalysts are presented in Table 2. As can be seen, none of the catalysts is fully reduced after the reduction treatment. Moreover, the NiZrAl and NiCaAl presented higher DOR's than the other catalysts, fact that could be inferred from the TPR profiles. The NiO particle size estimated by XRD is also presented in Table 2. As can be seen, all the catalysts present similar NiO crystallites ranging between 10 and 14 nm. It may be noted that the NiZrAl and NiCaAl presented the largest mean NiO crystallite sizes which could explain their slightly higher DOR's. Nevertheless, it is also possible that these promoters enhance the catalyst reducibility.

The metal dispersion of the catalysts and the estimated average Ni particle size are shown in Table 2. All catalysts are characterized by a relatively low metal dispersion as can be expected from catalysts containing high Ni loadings.

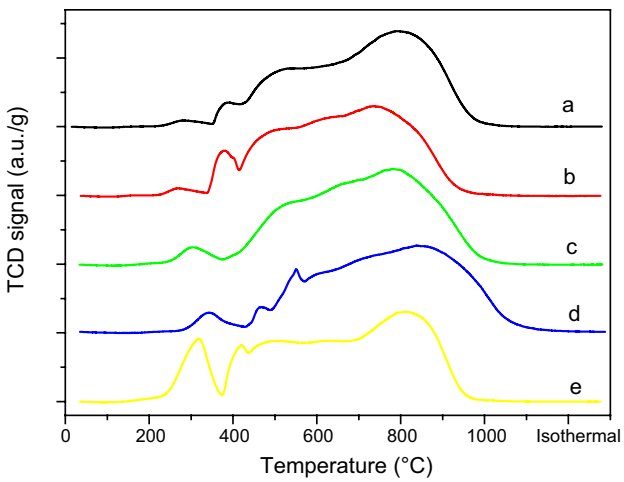

Fig. 1 Temperature programmed reduction (TPR) of the calcined catalysts using a flow consisting of 5% H_2 in Ar. *a* NiAl, *b* NiZrAl, *c* NiMgAl, *d* NiBaAl and *e* NiCaAl

Table 2 Physicochemical properties of the fresh catalysts

Catalyst	DOR (%)[a]	$d(NiO)_{XRD}$ (nm)[b]	$d(Ni)_{XRD}$ (nm)[c]	D (%)[d]	$d(Ni)_H$ (nm)[e]
NiAl	62	10	10	5.8	10
NiZrAl	86	14	11	5.5	15
NiMgAl	68	12	7	5.4	11
NiBaAl	74	11	8	7.3	10
NiCaAl	80	13	9	6.4	12

[a]Degree of reduction as estimated by H_2-TPR after catalyst reduction at 500 °C for 4 h in pure H_2 flow

[b]Average NiO particle size as estimated by XRD after catalyst calcination

[c]Average Ni particle size as estimated by XRD after catalyst reduction and passivation in air

[d]Metal dispersion as estimated by H_2 chemisorption after in situ catalyst reduction

[e]Average Ni particle size as estimated by H_2 chemisorption

Moreover, the NiBaAl and NiCaAl present slightly higher metal dispersion than the other catalysts. The average Ni particle size, as estimated by H_2 chemisorption, varies between 10 and 12 nm for all the catalysts except for the NiZrAl which presents a Ni particle size of ca. 15 nm. The particle sizes estimated by H_2 chemisorption slightly differ from those estimated by XRD. A possible explanation to this discrepancy may be the wrong assumption that the particles are spherical. Another explanation is the fact that the catalysts analyzed by XRD have been reduced and passivated in air. Indeed, the values obtained by H_2 chemisorption are slightly lower than those obtained by XRD, which may be explained by the oxidation or passivation of small Ni nanoparticles when the catalysts get in contact with air. Nonetheless, the Ni particle size estimated by XRD meets that determined by H_2 chemisorption in the case of the non-promoted catalyst. This incongruence may be ascribed to the precision of the instruments. It may also be mentioned that the thickness of the NiO layer around the Ni crystals may not be identical for all the catalysts. Unfortunately, the NiO layer surrounding the crystals is too thin [38] and was not detected with XRD.

3.2 Carbon Formation

The results obtained in the low-temperature CO methanation tests are summarized in Table 3. Apparently, any of the promoters has a clear positive effect on catalyst activity, at these reaction conditions. The catalysts lost between 23 and 27% of their activity in 24 h. The selectivity to CO_2, CH_4, C2, C3 and C4 hydrocarbons was, however, nearly constant during the tests. The selectivity to different hydrocarbons was very similar for all the catalysts except for the "NiCa". The "NiCa" presented a relatively high selectivity to CO_2 and a low selectivity to CH_4 compared to other catalysts. A possible explanation to this higher selectivity to CO_2 is that CaO increases the catalyst water gas shift activity. Another explanation could be that CaO favors the Boudouard reaction and thus, enhances both the formation of carbon and CO_2.

As explained previously, the reaction was stopped after 24 h and the carbon formed on the spent catalysts was analyzed by in situ temperature programmed hydrogenation. The results from the TPH analyses are presented in Fig. 2. The profiles reveal the existence of two peaks. These peaks are assigned to two different carbon species according to the work of McCarthy and Wise [39]. The first carbon species, hydrogenating between 100 and 200 °C, is assigned to atomic carbon or to strongly chemisorbed CO [40–42]. The second carbon species, hydrogenating between 400 and 600 °C is assigned to polymeric carbon. This carbon species, also called "C_β" or "gum", is responsible for deactivation [4, 34, 39, 40, 43].

The results from the GC analyses of the exit gas revealed that methane was the only hydrocarbon formed via carbon hydrogenation during the TPH analyses. This observation allowed the authors to quantify the amount of carbon using the methane TPH profiles. These quantitative results are presented in Fig. 3. The results show that the addition of Mg, Ca and Ba increase the amount of carbon formed. Contrariwise, the addition of Zr seems to reduce the carbon formation rate. The results are also presented in terms of "atoms of C/Ni active site" using the metal dispersion obtained by H_2 chemisorption. By evaluating the results

Table 3 Activity and selectivity of the catalysts during the low-temperature CO methanation tests

Catalyst	CO conversion (%)		SCH_4 (%)	SC_2 (%)	SC_3 (%)	SC_4 (%)	SCO_2 (%)
	Initial	After 24 h					
Ni	24.6	18.7	83.4	9.2	4.9	1.5	1.0
NiZr	25.0	19.2	82.4	9.4	5.5	1.7	1.0
NiMg	20.5	15.8	83.5	8.7	4.9	1.5	1.4
NiBa	26.0	19.0	83.4	8.9	4.9	1.5	1.3
NiCa	21.0	15.6	80.8	9.1	5.4	1.8	3.0

The reported selectivity values have been normalized. The maximum observed C-mass balance error was 1%

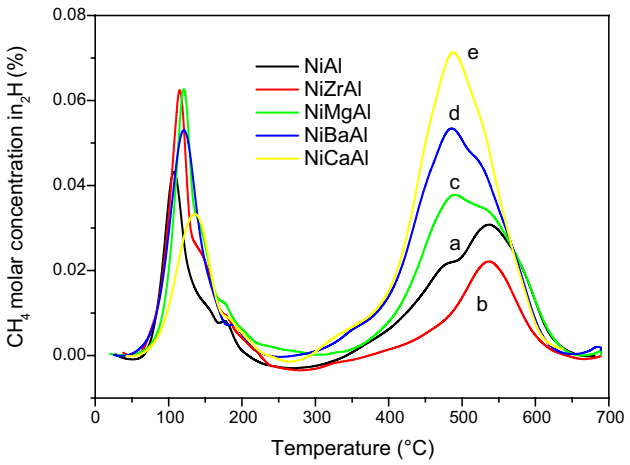

Fig. 2 TPH profiles of the spent catalysts after reaction at 300 °C, 1 bar and inlet H_2/CO =3. *a* NiAl, *b* NiZrAl, *c* NiMgAl, *d* NiBaAl and *e* NiCaAl

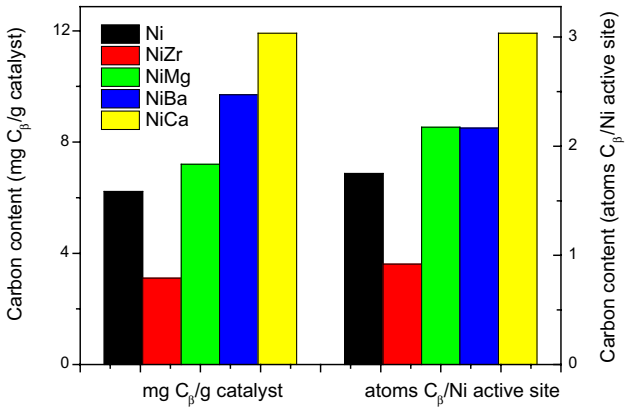

Fig. 3 Polymeric carbon (C_β) formed per unit mass of catalyst (*left*) and atoms of C_β formed per Ni active site (*right*). The latter was calculated using the metallic dispersion obtained from H_2-static chemisorption

in this manner, it can be concluded that the amount of carbon formed per Ni area is similar for the NiAl, NiMgAl and NiBaAl catalysts. Nevertheless, it cannot be discarded that the addition of Ca enhances the formation of carbon. Finally, it can be concluded that promotion with ZrO_2 can diminish the carbon formation rate, as suggested in previous studies [19–22]. The results encourage the performance of long tests in order to confirm that Zr inhibits carbon formation and reduces the catalyst deactivation rate.

3.3 Thermal Sintering

As explained in "experimental", the catalysts were aged at 690 °C in a H_2O/H_2 atmosphere for 7 days. In order to evaluate the loss of activity, the fresh and aged samples were tested at very mild conditions (H_2/CO =9, 1 bar and 300 °C). The methane yields of the fresh and aged samples are presented in Fig. 4 together with their respective Ni surface area. As can be seen, all the catalysts deactivate after the ageing treatments. Indeed, the loss of activity is almost complete after ageing at 30 bars. Moreover, as can be deduced from the figure, the loss of activity is explained by a loss of Ni surface area.

It may be noticed that, under these operating conditions (H_2/CO =9) all the promoters presented a positive effect on the initial catalyst activity. These results are surprising since no activity enhancement was observed in the carbon formation study when a H_2/CO =3 was employed (see Table 3). Apparently, these promoters only enhance the activity of Ni/γ-Al_2O_3 catalysts when using H_2-rich synthesis gas.

The proposed explanations for the loss of Ni surface area at these conditions are usually sintering of the Ni particles and pore collapse, the latter leading to the encapsulation of Ni particles [4, 8, 15, 16]. Another possible explanation is the oxidation of Ni nanoparticles. However, the risk for oxidation should be insignificant under these operating conditions [8, 44]. In order to assess if Ni oxidation takes place, some H_2 chemisorption experiments were repeated on aged samples but reducing the catalysts at 800 °C. Nevertheless, no enhancement of the metallic surface area was observed. Therefore, we believe that Ni oxidation did not take place under the ageing conditions.

In order to better comprehend these results the aged samples were analyzed by XRD and by N_2 adsorption. The NiO phase was not detected in any of the diffractograms which supports that oxidation of the Ni particles did not occur. The Ni particle size and pore size distribution of the fresh and aged catalysts are presented in Fig. 5. As can be seen, the Ni particle size increases after the accelerated ageing tests. It should be noted that, for some of the catalysts, the difference in Ni particle size between the ageing treatment at 1 and 30 bar is quite small, fact that suggests that the loss of Ni surface area is not only caused by a growth of the Ni particles. Moreover, the pore size distribution of all the catalysts changes after the ageing treatment. As can be seen in Fig. 5, there is a partial disappearance of small mesopores after the ageing treatment. Hence, it is likely that the loss of Ni surface area is also caused, to some extent, by sintering of the support and pore collapse.

In conclusion, the loss of activity under high temperatures and high steam pressures is attributed to sintering of both the Ni particles and the carrier. This extreme loss of activity found for the NiAl catalyst is in line with the results showed by Nguyen et al. [8] with a Ni/γ-Al_2O_3 catalysts with similar physicochemical properties. Moreover, none of these promoters led to a decent improvement of the catalyst thermal resistance. The results may be surprising since previous studies [19, 21, 22] claimed that Zr, for instance,

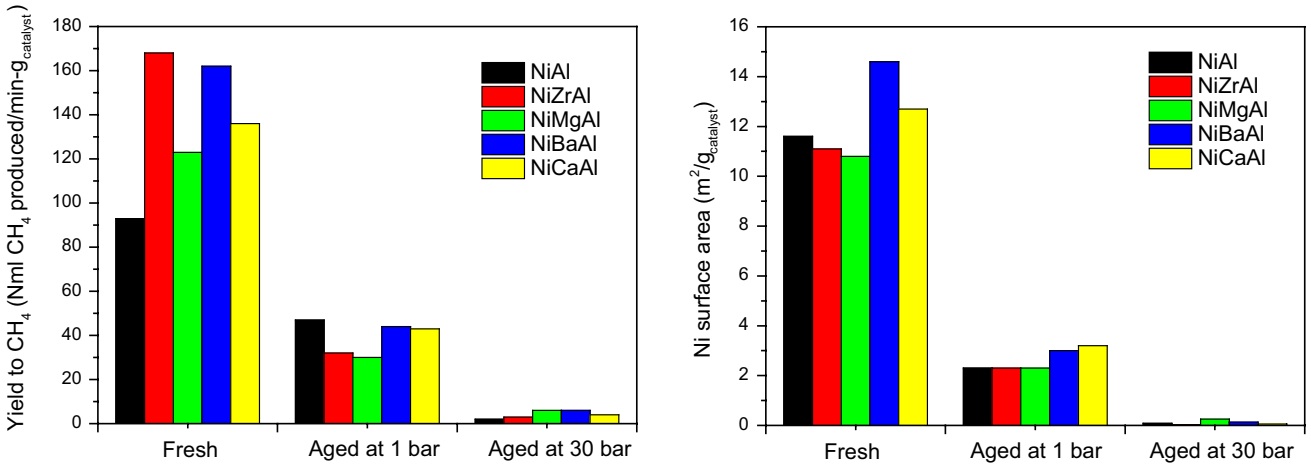

Fig. 4 Activity of the fresh and aged catalysts (*left*). Nickel surface area of the fresh and aged catalysts as estimated by H_2-chemisorption after in situ reduction at 500 °C for 4 h (*right*)

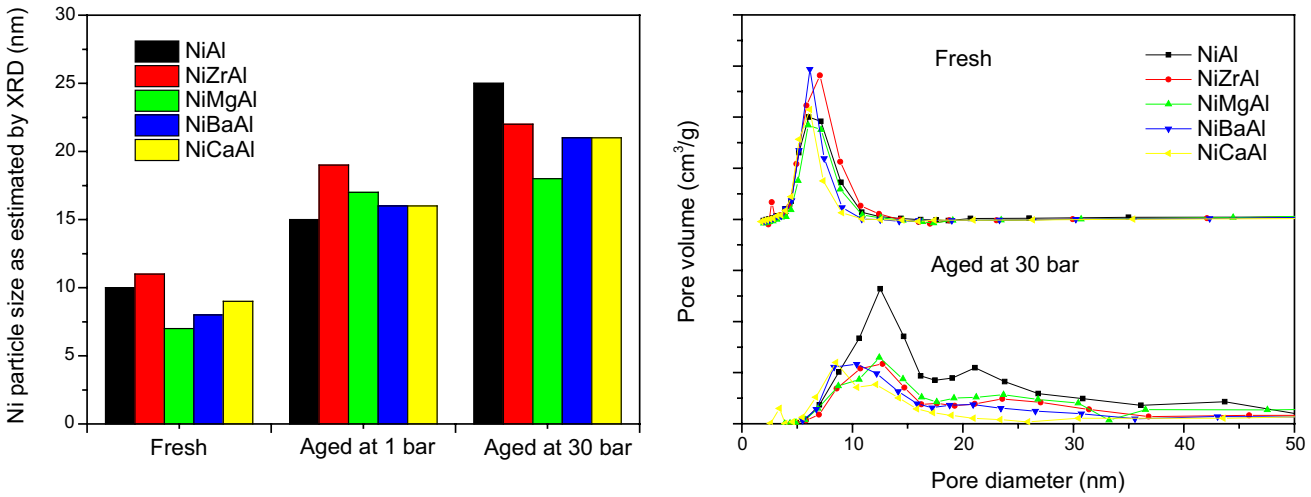

Fig. 5 Ni particle size of the fresh and aged catalysts (*left*). Pore size distribution of the fresh and aged catalysts (*right*)

enhanced the catalyst thermal stability. However, none of these studies exposed the catalysts to such high temperatures and steam partial pressures. It may be noted that the ageing conditions employed in this work are defined according to the current operability of commercial nickel-based methanation catalysts [8]. It is certain that our ageing results at 30 bar indicate that the growth of the Ni particles is largest for the NiAl catalyst. Nevertheless, the growth of the Ni particles could have been limited by the support pore structure rather than by the presence of these promoters. Therefore, it is not clear whether these promoters restrain the growth of the Ni crystals. The use of pre-stabilized alumina carriers with wider pores is recommended for clarifying this possible effect of these promoters and also to avoid sintering of the support and encapsulation of Ni particles.

4 Conclusions

In the present work, a series of alumina-supported nickel catalysts promoted with low amounts of Zr, Mg, Ba or Ca oxides were prepared in order to evaluate their resistance to carbon formation and thermal sintering under methanation conditions. For that purpose, the catalysts were tested under low temperature CO methanation conditions favorable for the formation of polymeric carbon. Furthermore, the catalysts were aged at high temperatures and high steam partial pressures in order to evaluate their thermal stability.

The catalysts lost practically all their activity after the ageing treatments. The loss of activity was explained by a loss of Ni surface area. The loss of metal surface area was ascribed to sintering of the Ni particles and pore collapse.

The use of these promoters was apparently not a convenient solution to improve the thermal resistance of high surface area Ni/Al_2O_3 catalysts. Nonetheless, ZrO_2 was found to be an effective promoter to reduce the carbon formation rate. The addition of CaO had however an adverse effect on carbon formation. Future work could address the use of ZrO_2 on pre-stabilized alumina carriers in order to avoid sintering of the support and encapsulation of Ni particles.

Acknowledgements The research leading to these results has received funding from the European Union Seventh Framework Programme (FP7/2013) under Grant Agreement No. 308733.

References

1. Kopyscinski J, Schildhauer TJ, Biollaz SMA (2010) Production of synthetic natural gas (SNG) from coal and dry biomass—A technology review from 1950 to 2009. Fuel 89:1763–1783
2. Senanayake SD, Evans J, Agnoli S, Barrio L, Chen T-L, Hrbek J, Rodriguez JA (2011) Water–Gas shift and CO methanation reactions over Ni–CeO2(111) catalysts. Top Catal 54:34–41
3. Höhlein B, Niessen H, Range J, Schiebahn HJR, Vorwerk M (1984) Methane from synthesis gas and operation of high-temperature methanation. Nucl Eng Des 78:241–250
4. Pedersen K, Skov A, Rostrup-Nielsen JR (1980) Catalytic aspects of high temperature methanation. ACS Div Fuel Chem 25:89–100 (Preprints)
5. Sehested J, Larsen KE, Kustov AL, Frey AM, Johannessen T, Bligaard T, Andersson MP, Nørskov JK, Christensen CH (2007) Discovery of technical methanation catalysts based on computational screening. Top Catal 45:9–13
6. Gao J, Wang Y, Ping Y, Hu D, Xu G, Gu F, Su F (2012) A thermodynamic analysis of methanation reactions of carbon oxides for the production of synthetic natural gas. RSC Adv 2:2358–2368
7. Watson GH, Research IC (1980) Methanation Catalysts. IEA Coal Research
8. Nguyen TTM, Wissing L, Skjøth-Rasmussen MS (2013) High temperature methanation: Catalyst considerations. Catal Today 215:233–238
9. Rönsch S, Schneider J, Matthischke S, Schlüter M, Götz M, Lefebvre J, Prabhakaran P, Bajohr S (2016) Review on methanation—From fundamentals to current projects. Fuel 166:276–296
10. Williams A, Butler GA, Hammonds J (1972) Sintering of nickel-alumina catalysts. J Catal 24:352–355
11. Rostrup-Nielsen JR, Pedersen K, Sehested J (2007) High temperature methanation. Sintering and structure sensitivity. Appl Catal A 330:134–138
12. Bartholomew CH (2001) Mechanisms of catalyst deactivation. Appl Catal A 212:17–60
13. Shen WM, Dumesic JA, Hill CG Jr (1981) Criteria for stable Ni particle size under methanation reaction conditions: Nickel transport and particle size growth via nickel carbonyl. J Catal 68:152–165
14. Barrientos J, González N, Lualdi M, Boutonnet M, Järås S (2016) The effect of catalyst pellet size on nickel carbonyl-induced particle sintering under low temperature CO methanation. Appl Catal A 514:91–102
15. Bartholomew CH, Pannell RB, Fowler RW (1983) Sintering of alumina-supported nickel and nickel bimetallic methanation catalysts in H2/H2O atmospheres. J Catal 79:34–46
16. Gao J, Jia C, Li J, Zhang M, Gu F, Xu G, Zhong Z, Su F (2013) Ni/Al_2O_3 catalysts for CO methanation: effect of Al_2O_3 supports calcined at different temperatures. J Energy Chem 22:919–927
17. Rostrup-Nielsen JR, Pedersen K, Jorn E, Skov A (1981) A method and catalyst for exothermal catalytic gas phase reactions. Patent GB2077613A
18. Gao J, Liu Q, Gu F, Liu B, Zhong Z, Su F (2015) Recent advances in methanation catalysts for the production of synthetic natural gas. RSC Adv 5:22759–22776
19. Meng F, Li Z, Ji F, Li M (2015) Effect of ZrO_2 on catalyst structure and catalytic methanation performance over Ni-based catalyst in slurry-bed reactor. Int J Hydrogen Energy 40:8833–8843
20. Liu Q, Gu F, Gao J, Li H, Xu G, Su F (2014) Coking-resistant $Ni\text{-}ZrO_2/Al_2O_3$ catalyst for CO methanation. J Energy Chem 23:761–770
21. Liu Q, Gu F, Zhong Z, Xu G, Su F (2016) Anti-sintering ZrO_2-modified $Ni/\alpha\text{-}Al_2O_3$ catalyst for CO methanation. RSC Adv 6:20979–20986
22. Guo C, Wu Y, Qin H, Zhang J (2014) CO methanation over ZrO_2/Al_2O_3 supported Ni catalysts: a comprehensive study. Fuel Process Technol 124:61–69
23. Rotgerink HGJL, Paalman RPAM, van Ommen JG, Ross JRH (1988) Studies on the promotion of nickel—alumina coprecipitated catalysts. Appl Catal 45:257–280
24. Fan MT, Miao KP, Lin JD, Zhang HB, Liao DW (2014) Mg-Al oxide supported Ni catalysts with enhanced stability for efficient synthetic natural gas from syngas. Appl Surf Sci 307:682–688
25. Liu J, Yu J, Su F, Xu G (2014) Intercorrelation of structure and performance of $Ni\text{-}Mg/Al_2O_3$ catalysts prepared with different methods for syngas methanation. Catal Sci Technol 4:472–481
26. Alipour Z, Rezaei M, Meshkani F (2014) Effect of alkaline earth promoters (MgO, CaO, and BaO) on the activity and coke formation of Ni catalysts supported on nanocrystalline Al_2O_3 in dry reforming of methane. J Ind Eng Chem 20:2858–2863
27. Alipour Z, Rezaei M, Meshkani F (2014) Effects of support modifiers on the catalytic performance of Ni/Al_2O_3 catalyst in CO_2 reforming of methane. Fuel 129:197–203
28. Lemaitre JL, Delannay F (1984) Characterization of heteogeneous catalysts. Marcel Dekker, New York
29. Bartholomew CH, Farrauto RJ (2010) Fundamentals of industrial catalytic processes, 2nd edn. Wiley, Hoboken
30. Weisz PB, Hicks JS (1962) The behaviour of porous catalyst particles in view of internal mass and heat diffusion effects. Chem Eng Sci 17:265–275
31. Borg Ø, Eri S, Blekkan EA, Storsæter S, Wigum H, Rytter E, Holmen A (2007) Fischer–Tropsch synthesis over γ-alumina-supported cobalt catalysts: effect of support variables. J Catal 248:89–100
32. Storsæter S, Borg Ø, Blekkan EA, Holmen A (2005) Study of the effect of water on Fischer–Tropsch synthesis over supported cobalt catalysts. J Catal 231:405–419
33. Lualdi M (2012) Fischer–Tropsch synthesis over cobalt-based catalysts for BTL applications. Kungliga Tekniska Högskolan. Doctoral thesis
34. Moodley DJ, van de Loosdrecht J, Saib AM, Overett MJ, Datye AK, Niemantsverdriet JW (2009) Carbon deposition as

a deactivation mechanism of cobalt-based Fischer–Tropsch synthesis catalysts under realistic conditions. Appl Catal A 354:102–110
35. Rynkowski JM, Paryjczak T, Lenik M (1993) On the nature of oxidic nickel phases in NiO/γ-Al_2O_3 catalysts. Appl Catal A 106:73–82
36. Vogelaar BM, van Langeveld AD, Kooyman PJ, Lok CM, Bonné RLC, Moulijn JA (2011) Stability of metal nanoparticles formed during reduction of alumina supported nickel and cobalt catalysts. Catal Today 163:20–26
37. Zieliński J (1993) Effect of alumina on the reduction of surface nickel oxide; morphology of the surfaces of the surfaces of Ni/Al_2O_3 catalysts. J Mol Catal 83:197–206
38. Shido T, Lok M, Prins R (1999) Characterization of highly dispersed Ni/Al_2O_3 catalysts by EXAFS analysis of higher shells. Top Catal 8:223–236
39. McCarty JG, Wise H (1979) Hydrogenation of surface carbon on alumina-supported nickel. J Catal 57:406–416
40. Bartholomew CH (1982) Carbon deposition in steam reforming and methanation. Catal Rev 24:67–112
41. Wentrcek PR, McCarty JG, Wood BJ, Wise H (1976) Formation of surface carbon and methanation catalysis on alumina supported nickel. Am Chem Soc Div Fuel Chem Prepr 21:52–63
42. Mirodatos C, Dalmon JA, Martin GA (1984) Nature and role of carbon species during CO and CO-H_2 reactions over Ni/SiO_2 catalysts. Stud Surf Sci Catal 19:505–512. doi:10.1016/S0167-2991(09)60135-X
43. Saib AM, Moodley DJ, Ciobîcă IM, Hauman MM, Sigwebela BH, Weststrate CJ, Niemantsverdriet JW, van de Loosdrecht J (2010) Fundamental understanding of deactivation and regeneration of cobalt Fischer-Tropsch synthesis catalysts. Catal Today 154:271–282
44. Rostrup-Nielsen JR (1984) Catalytic steam reforming. Catalysis 5:1–117